Above Cloud CCN Concentrations Help to Sustain Some Arctic Low-Level Clouds

Lucas J. Sterzinger[1,2,3] and Adele L. Igel[1]

[1]Department of Land, Air and Water Resources, University of California, Davis, Davis, California, USA
[2]NASA Goddard Space Flight Center, Greenbelt, Maryland, USA
[3]ADNET Systems, Inc, Bethesda, Maryland, USA

Correspondence: Adele L. Igel (aigel@ucdavis.edu)

Abstract. Previous studies have found that low-level Arctic clouds often persist for long periods even in the face of very low surface cloud condensation nuclei (CCN) concentrations. Here we investigate whether these conditions could occur due continuous entrainment of aerosol particles from the free troposphere. We use an idealized LES modeling framework where aerosol concentrations are low in the boundary layer, but increased up to 50x in the free troposphere. We find that the tests with higher tropospheric aerosol concentrations simulated clouds which persisted for longer and maintained higher liquid water paths. This is due to direct entrainment of the tropospheric aerosol into the cloud layer which results in a precipitation suppression from the increase in cloud droplet number and in stronger cloud top radiative cooling, which causes stronger circulations maintaining the cloud in the absence of surface forcing. Together, these two responses result in a more well-mixed boundary layer with a top that remains in contact with the tropospheric aerosol reservoir and can maintain entrainment of those aerosol particles. The surface aerosol concentrations, however, remained low in all simulations. The free tropospheric aerosol concentration necessary to maintain the clouds is consistent with concentrations that are frequently seen in observations.

1 Introduction

Low level mixed-phase clouds are crucial regulators of Arctic climate (Intrieri et al., 2002; Shupe and Intrieri, 2004; Sedlar et al., 2011) and are ubiquitous (Shupe et al., 2006, 2011; Shupe, 2011). Properly modeling these clouds is necessary to accurately project Arctic and global climate change, yet representation of Arctic low-level clouds in models has remained a challenge. (Klein et al., 2009; Morrison et al., 2009, 2011, 2012; Sotiropoulou et al., 2016). Low-level Arctic clouds have been observed to exist for days at a time (Shupe, 2011; Shupe et al., 2011; Morrison et al., 2012; Verlinde et al., 2007). This is especially curious given the low aerosol concentrations in the Arctic; boundary layer aerosol concentrations are at a minimum in the summer (Mauritsen et al., 2011; Heintzenberg et al., 2015) with typical accumulation mode concentrations less than 100 cm^{-3} and sometimes less than 1 cm^{-3}. Such low concentrations may be insufficient to maintain clouds (Mauritsen et al., 2011; Stevens et al., 2018; Sterzinger et al., 2022).

One idea regarding how these low-level clouds can be maintained in the face of such low accumulation mode concentrations is that Aitken mode particles become important for cloud droplet activation (Bulatovic et al., 2021). This idea is supported by observational evidence suggesting that Aitken particles contribute to CCN populations in the Arctic (Willis et al., 2016; Koike

et al., 2019; Kecorius et al., 2019) and in many cases even dominate the CCN population (Karlsson et al., 2021, 2022; Siegel et al., 2022). The importance of the Aitken mode for cloud droplets has also been suggested in Southern Ocean low-level clouds (McCoy et al., 2021). The observations are supported by large eddy simulations and show that supersaturation in these low-level high latitude clouds can be large enough to activate Aitken particles (Bulatovic et al., 2021; Wyant et al., 2022). However, Bulatovic et al. (2021) found that when Aitken mode concentrations are low, the accumulation mode concentrations are most likely also low. That is, when accumulation mode concentrations are low, there may not necessarily be enough Aitken particles to sustain the low-level clouds either.

It has also been shown that measurements taken at the surface may not be representative of the rest of the lower atmosphere. Aerosol concentrations have been observed to be higher in the free troposphere (FT) than in the boundary layer (BL) (Lonardi et al., 2022; Creamean et al., 2021; Wylie and Hudson, 2002; Hegg et al., 1995; Igel et al., 2017). More specifically, using tethered balloon data from Oliktok Pt, Alaska spanning late spring 2017 through early fall 2018, Creamean et al. (2021) found that above cloud aerosol concentrations were higher than those below cloud in 38% of profiles analyzed. Lonardi et al. (2022) and Igel et al. (2017), using summertime data from the high Arctic, similarly found higher concentrations of tropospheric aerosol concentrations when compared to the surface, but these studies presented data from a limited number of days (four days in Igel et al. (2017) and three days in Lonardi et al. (2022), both over a week and a half timeframe).

It has been found that entrainment of aerosol particles above the inversion can be an important source of aerosol for the Arctic boundary layer (Igel et al., 2017; Price et al., 2023). As such, while the activation of Aitken particles may be one way to maintain low-level clouds when accumulation mode particle concentrations are ultra-low, the continuous entrainment of accumulation mode particles at cloud top may be another way.

In this study, we first analyze the entire tethered balloon dataset from MOSAiC (Pilz et al., 2022a) for further evidence that enhanced aerosol concentrations frequently exist above the boundary layer top and to determine whether there are any consistent changes in the size distribution across the boundary layer top. We then use idealized modeling to investigate the sensitivity of Arctic mixed-phase boundary layer clouds to aerosol concentrations in the free troposphere - specifically aerosol that can act as cloud condensation nuclei. We present a suite of simulations, each with different tropospheric aerosol concentrations and examine the effect of these varied concentrations on aerosol, cloud, and boundary layer properties. Finally, we briefly examine the sensitivity of our results to thermodynamic conditions.

2   Tethered Balloon Observations

Here we extend the analysis presented by Lonardi et al. (2022) to include all BELUGA (Balloon-bornE moduLar Utility for profilinG the lower Atmosphere) tethered balloon profiles from the high Arctic collected during MOSAiC (Shupe et al., 2022) with a well-defined temperature inversion to mark the transition to the free troposphere that is at least 100m below the profile top (Pilz et al., 2022b). We identified eight balloon flights that meet these criteria, only two of which were shown in Lonardi et al. (2022) (23 July 2020 beginning at 0901 UTC and 24 July 2020). These flights occur over about one month. Coincident measurements of cloud presence (Lonardi et al., 2022b) and radiation properties (Lonardi et al., 2022a) with the
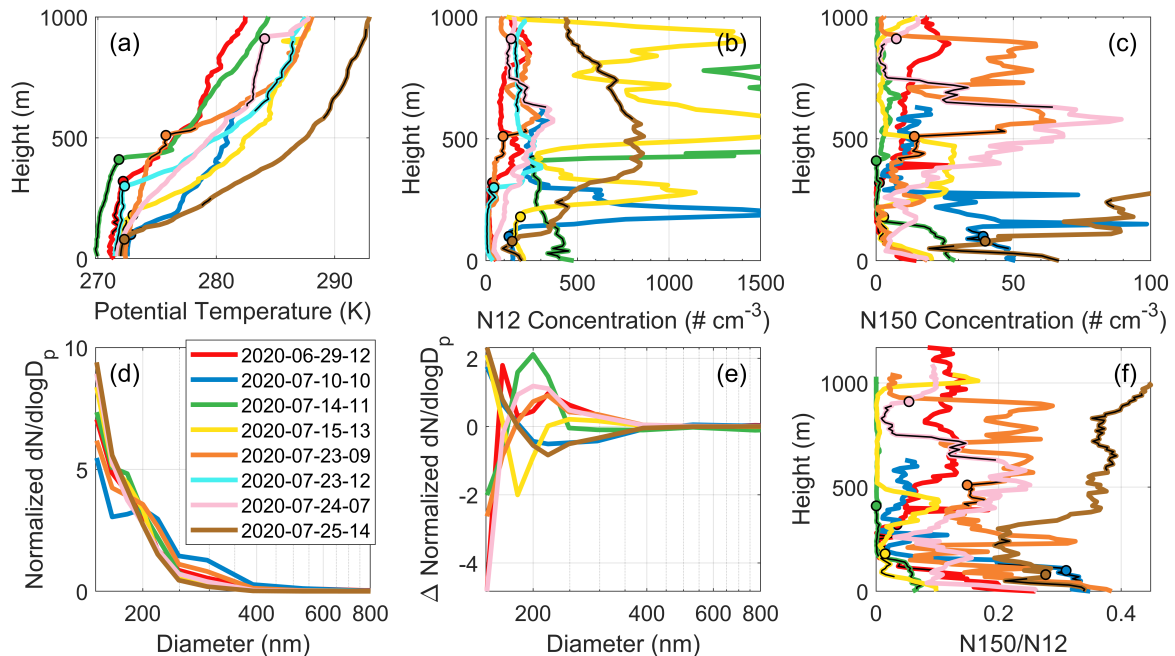
Figure 1. Profiles of (a) potential temperature, (b) concentration of particles with diameter >12 nm (N12), (c) concentration of particles with diameter >150 nm (N150), and (f) the ratio of N150 to N12 for select tethered balloon flights during the MOSAiC campaign. Black outlined circles represent the top of the mixed layer for each profile. Thin black lines indicate the most likely location of a cloud layer. (d) Normalized distributions averaged over 100m above the mixed layer top and (e) the normalized size distribution averaged over 100 m above the mixed layer top minus the normalized size distribution averaged 100 m below the mixed layer top.

aerosol concentration measurements (Pilz et al., 2022a) are typically not available, but are instead frequently available an hour or two prior to the collection of the aerosol data. We use a combination of the cloud presence flags (available for only two
60   flights), the broadband fluxes, and the relative humidity to make a best guess at the extent of cloud layers for each aerosol data flight. Typically these layers seem consistent with the potential temperature profiles despite the measurements not be coincident in time (1a). Figure 1a-c shows vertical profiles of potential temperature and aerosol concentration for particle diameters >12 nm (N12) and >150 nm (N150) for all eight identified flights. Flight data has been binned and averaged over 10m height bins. The extent of the cloud layers is shown with overlaid thin black lines. Note that even though cloud layers are identified, the
65   aerosol measurements may or may not have occurred in clear skies.

    All aerosol profiles (Fig. 1b) have higher N12 concentrations above the inversion than at any level below the inversion with the exception of 24 July 2020. The N150 data is noisier; most profiles do show higher concentrations just above the inversion compared to below, but this could just be the result of aerosol scavenging by the cloud layer, such as is possibly evident on 29 June, 14 July, and/or 15 July. While the N150 data are more relevant for cloud droplet activation, there is growing evidence that

70 Aitken mode particles contribute to droplet formation in environments with low accumulation mode concentration (Karlsson et al., 2021, 2022; Siegel et al., 2022). Therefore, both the N12 and N150 profiles are relevant for cloud layers in the Arctic. Some profiles show free-tropospheric N12 aerosol concentrations in the low 100s cm^{-3}, while others are seen to reach 1000 cm^{-3} or more. In all but one profile, the N150 concentrations are less than 100 cm^{-3} throughout the lowest 1km of the atmosphere. In all profiles, near-surface N12 aerosol concentrations were quite low, most below 200 cm^{-3} and some well

75 below 100 cm^{-3}, despite the higher concentrations in the free troposphere. Although the number of in situ observations of above-inversion aerosol concentrations in the high Arctic remains low, there is increasing evidence that the concentration of aerosol particles is higher above immediately above the inversion than at the surface more often than not during the summer months.

We can also examine the size distribution of aerosol particles for particles with diameters >150 nm with the BELUGA data.
80 The normalized size distributions averaged over the 100m above the mixed layer top show that the modal diameter in all cases is 150 nm or less (Fig. 1d). As such, from this data alone, it is difficult to determine a mean aerosol particle size. Nonetheless, we can take a difference in the normalized distributions averaged over 100 m above and below the mixed layer top to get a sense for whether there is a shift in the size distributions (Fig. 1e). Doing so reveals that there is no consistent trend among the flights; in some cases, the relative number of the smallest particles (sizes near 150 nm) increase and the relative number of
85 larger particles decrease whereas in other cases the opposite is true. Likewise, there is no consistent trend in the ratio of N150 to N12 as a function of height (Fig. 1f). In the model simulations that follow, we will assume that there is no change in the mean size of the aerosol population across the boundary layer top.

3   Model Simulations

We used the Colorado State University Regional Atmospheric Modeling System (RAMS; Cotton et al., 2003) to run large eddy
90 simulations of Arctic low-level clouds. RAMS uses a double-moment bulk microphysics scheme (Meyers et al., 1997; Saleeby and Cotton, 2004) predicting hydrometeor mass and number concentrations for cloud, rain, ice, snow, aggregates, graupel, and hail. The scheme includes a prognostic aerosol treatment (Saleeby and van den Heever, 2013) which prognoses the aerosol mass and number concentrations. When aerosol particles activate to form droplets or ice crystals, the aerosol mass is tracked within the hydrometeor categories. Cloud droplets are activated from aerosol particles using Köhler theory by referencing
95 lookup tables (Saleeby and Cotton, 2004) and hydrometeor diffusional growth is explicitly dependent on supersaturation. Dry and wet deposition of aerosols is included (Saleeby and van den Heever, 2013), but new particle formation is not parameterized in the RAMS aerosol scheme. Ice nucleation is parameterized following DeMott et al. (2010) as described in Saleeby and van den Heever (2013). Aerosol particles are regenerated upon hydrometeor evaporation and the aerosol mass returned to the atmosphere is proportional to the fraction of hydrometeor mass that was fully evaporated.
100 In order to investigate the aerosol impacts on the liquid phase alone, the model was modified to have separate categories for aerosol able to act as cloud condensation nuclei (CCN) and ice nucleating particles (INP). Salt was chosen as the aerosol category that would only serve as CCN, as it is totally soluble and cannot act as INP. Dust was chosen as the aerosol acting

as INP; routines that allowed liquid nucleation onto dust were deactivated. While dust is known to act as CCN, the DeMott parameterization makes no distinction between immersion and deposition freezing - only the total number of particles, in or out of droplets, is required. Therefore, we think that this separation approach is appropriate. In this study, we are concerned solely with the impacts of CCN on mixed-phase Arctic clouds - this separation of CCN and INP will allow for future study on the impact of INP alone. Furthermore, most of the simulations in this study are run at temperatures that are only slightly supercooled; ice is negligible in these simulations and will not be discussed.

Longwave radiation is parameterized by BUGSRAD, a two-stream radiation model (Stephens et al., 2001) that includes a dependency on the effective radius of cloud droplets and ice crystals. Despite ultra-low aerosol concentrations typically occurring during the summer, we neglect shortwave radiation to avoid the complications of a diurnal cycle and to avoid needing to tie our simulations to a specific day of the year. Subgrid-scale turbulence and diffusion is based on Deardorff (1980) - this scheme parameterizes eddy viscosity as a function of resolved turbulent kinetic energy (TKE). Surface fluxes were set to zero to provide an idealized framework in which cloud processes can be examined without influence from the surface. The surface roughness length for momentum is set to 5×10^{-4}m. These surface assumptions are supported by observations of surface fluxes in the Arctic (Schröder et al., 2003).

The simulations in this study follow a similar setup to those in Sterzinger et al. (2022): a 6×6 km^2 periodic domain with 62.5 m horizontal and 6.25 m vertical grid spacing. Model top was set at 1500 m. Simulations were run for a simulated 30 hours with a 1 second time step. The model was initialized with analytic thermodynamic profiles. A recent analysis of MOSAiC data by Jozef et al. (2023) showed that in the Arctic summer, boundary layers with very shallow mixed layers less than 125m deep are about as common as deeper, near-neutral layers. Both are frequently associated with low clouds and both are most frequently capped by inversions of 5K per 100m or stronger. Our base setup, in terms of inversion strength and boundary layer stability, is consistent with this latter cloud-bearing regime. Analytic profiles rather than case-based profiles are chosen so as to be able to easily modify them in thermodynamic sensitivity tests which will be described below. These profiles (BASE) are given by:

$$
\theta(z) = \begin{cases} \theta_0, & z \leq 700 \text{ m} \\ \theta_0 + a(z-700), & 700 \text{ m} < z \leq 800 \text{ m} \\ \theta_0 + 100a + 0.005(z-800), & z > 800 \text{ m} \end{cases} \tag{1}
$$

$$
w(z) = \begin{cases} w_0, & z \leq 700\text{m} \\ w_0 + \frac{0.75w_s(800)-w_0}{100}(z-700), & 700\text{m} < z \leq 800\text{m} \\ \frac{0.75}{2}w_s(z)(e^{-\frac{z-800}{200}}+1), & z > 800\text{m} \end{cases} \tag{2}
$$

where z is the height above the surface in meters, θ is potential temperature, w is the water vapor mixing ratio, and w_s is the saturated mixing ratio. For the BASE simulation, $\theta_0 = 273.15$ K, $a = 0.06$ K m^{-1}, and w_0 is the mixing ratio that gives 100% relative humidity at cloud base. We use a cloud that is initially 150m thick, and as such, $w_0 = 2.7$ g kg^{-1}.
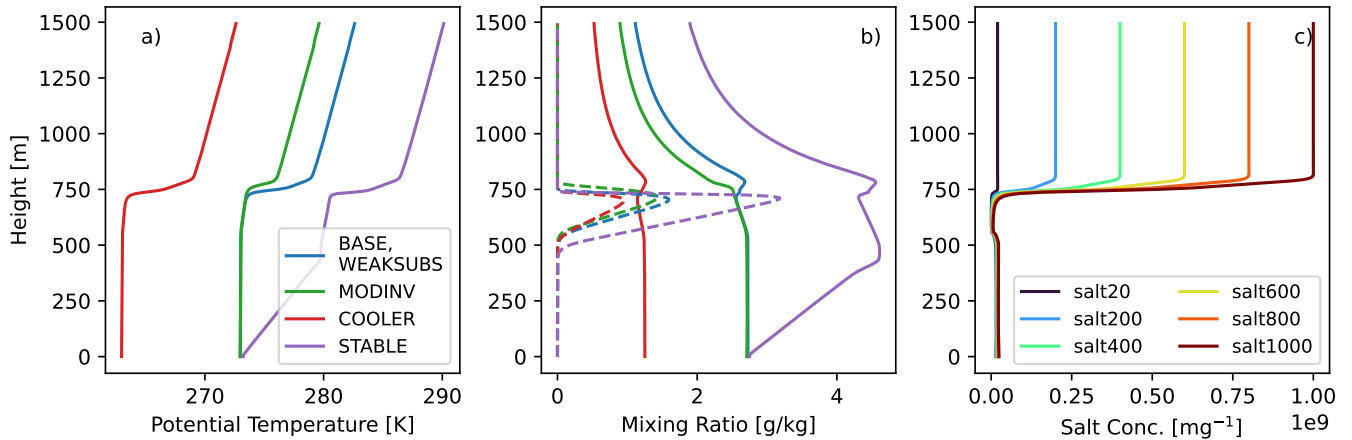
Figure 2. Profiles of (a) potential temperature, (b) water vapor mixing ratio (solid lines) and cloud water mixing ratio (dashed lines; multiplied by 10 for clarity), and (c) salt aerosol profiles taken 30 minutes after simulation initialization. Panels (a) and (b) show profiles for the base and thermodynamic sensitivity tests and panel (c) shows profiles for the salt experiments in the base setup.

We do not explicitly initialize cloud water. Instead, the potential temperature and water vapor profiles produce relative humidity well in excess of 100% in the cloud layer. Excess water vapor is converted to cloud water by the model and the associated latent heat of condensation is added to the temperature profile. Since it is these conditions - those after the model has modified the profiles that we provide in the input files - that are of most interest for understanding the model setup, we
135 show profiles of potential temperature, water vapor, and cloud mixing ratio shortly after model initialization in Figure 2a-b in blue. Winds are calm and nudging of the profiles to the initial condition is not performed. Large-scale subsidence prescribed by a fixed divergence rate of 6.0×10^{-6} s^{-1}. This value was chosen to prevent the boundary layer top from rising too rapidly.

To test the sensitivity to tropospheric CCN concentrations, a suite of simulations were run across a range of tropospheric salt concentrations. A baseline simulation with a salt aerosol particle concentration of 20 mg^{-1} at all levels was run. Sensitivity
140 tests were run in which salt concentrations in the FT were set by multiples of 200 mg^{-1} until a concentration of 1000 mg^{-1} (Fig. 2c). These concentrations were chosen to be representative of the range of observed aerosol concentrations in the Arctic troposphere, with 1000 mg^{-1} being a high, but not unrealistically high, value (Fig. 1b). The concentration in the inversion layer linearly increases with height from 20 mg^{-1} to the FT concentration. In all simulations, the aerosol particles were lognormally distributed with a modal diameter of 200 nm and a logarithmic standard deviation of 1.5. These parameters were kept constant
145 with height given that we found no consistent trends in the change in size across the mixed layer top (Fig. 1e-f). For all of these CCN sensitivity simulations, dust concentrations were set at 20 mg^{-1} in both the FT and BL.

Since salt concentrations are the only aerosol species being modified in this study, from this point forward any mention of 'aerosol' is in reference to salt/CCN particles alone unless specified otherwise.

Finally, to test the sensitivity of our conclusions to the initial thermodynamic profile, we run an additional set of simulations
150 with salt concentrations of 400 and 1000 mg^{-1} in the FT. These include tests in which the temperature inversion strength is

halved, that is, $a = 0.03$ K m^{-1} in Eq. 1 (MODINV, consistent with common "moderate" inversions found in Jozef et al. 2023), the surface temperature is decreased by 10K (COOLER, $\theta_0 = 263$K in Eq. 1), and a stable layer is introduced below the cloud layer (STABLE). The modified equations for the initial conditions in STABLE are given by:

$$\theta(z) = \begin{cases} \theta_0 + 0.015z, & z \leq 500 \text{ m} \\ \theta_0 + 7.5, & 500 \text{ m} < z \leq 700 \text{ m} \\ \theta_0 + 7.5 + a(z - 700), & 700 \text{ m} < z \leq 800 \text{ m} \\ \theta_0 + 7.5 + 100a + 0.005(z - 800), & z > 800 \text{ m} \end{cases} \tag{3}$$

$$w(z) = \begin{cases} w_0 - 4 \times 10^{-6}(700 - z), & z \leq 500 \text{ m} \\ w_0, & 500 \text{ m} < z \leq 700 \text{ m} \\ w_0 + \frac{0.75w_s(800) - w_0}{100}(z - 700), & 700 \text{ m} < z \leq 800 \text{ m} \\ \frac{0.75}{2} w_s(z)\left(e^{-\frac{z-800}{200}} + 1\right), & z > 800 \text{ m} \end{cases} \tag{4}$$

In all cases, the initial cloud layer is 150 m thick. In STABLE, the mixing ratio profile gives a relative humidity that is nearly identical to that in BASE. We note that in STABLE, because the surface potential temperature is the same as in BASE, the cloud layer itself is warmer than in BASE. Finally, simulations are run which are identical to BASE except that the subsidence rate is halved (WEAKSUBS). Thermodynamic profiles for all of these tests shortly after model initialization are shown in Figure 2a-b.

4 Model Simulation Results

4.1 Microphysical Response

The clouds produced by the six simulations are shown in Fig. 3. Clouds appear to have quasi-steady cloud tops for the higher aerosol concentration simulations (by design), with cloud top mixing ratios of around 0.35 g kg^{-1}. There is a strong sensitivity to FT aerosol concentration, with simulations initialized with FT salt concentrations of 20-400 mg^{-1} dissipating or nearly dissipating within 10-20 hours, while the simulations initialized with concentrations of 600 mg^{-1} or higher are able to persist for the entire simulation period - though salt600 is headed toward dissipation. Salt600, salt800 and salt1000 are similar for the first 10 hours or so but start to diverge after this time. All simulations produce some rain water (Fig. 4b). For salt800 and above, the rain water is a small fraction of the total liquid water. As seen by a lack of liquid water in the domain mean near the surface (Fig. 3), very little rain water actually reaches the surface. Surface precipitation rates are at most 1.2 mm per day, which is essentially negligible and not large enough to be observed. Rather, the vast majority of the little rain that exists is quickly evaporated below cloud base.
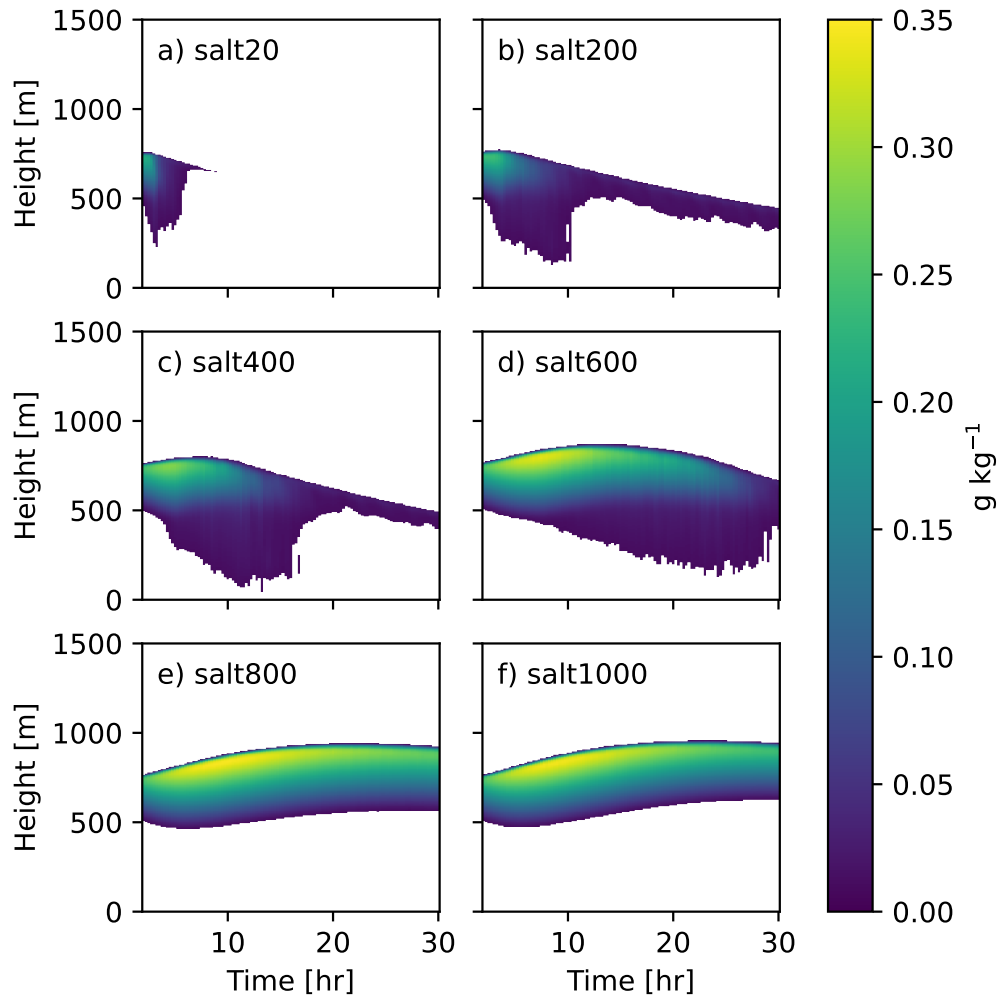
Figure 3. Time-height contours of total liquid water for all six base simulations. The minimum liquid water mixing ratio shown is 0.01 g kg^{-1}. The black line denotes a 0.01 g kg^{-1} contour of cloud water alone.
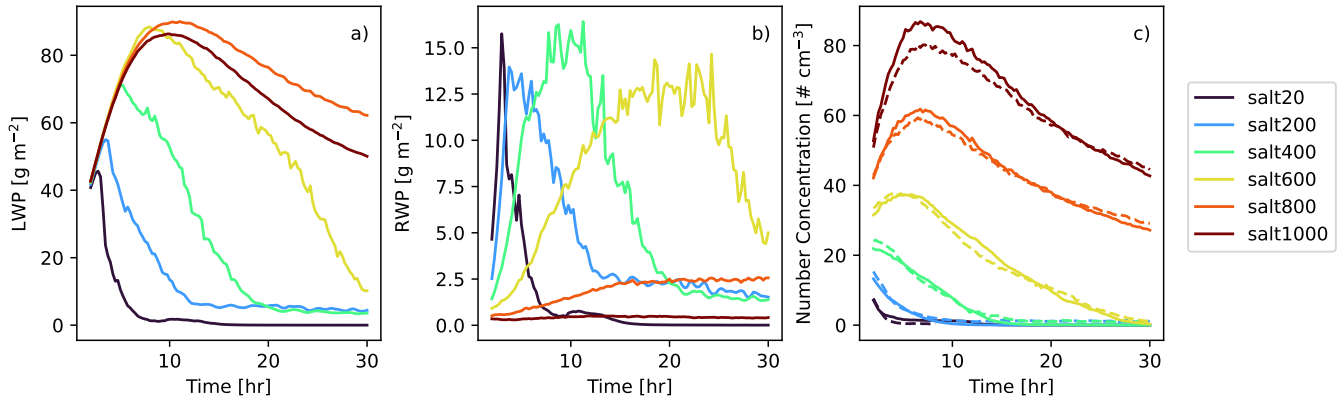
Figure 4. (a) Liquid water path, (b) rain water path for each base simulation, and (c) surface aerosol concentrations (solid) in the lowest model level and mean cloud droplet number concentrations (dashed) within the cloud layer. The first two hours are omitted.

Since the BL aerosol concentration is initialized to 20 mg^{-1} in all simulations, any changes in cloud liquid properties must come from tropospheric aerosol being entrained into the cloud layer. As such, we now look to how the boundary layer aerosol concentrations and droplet concentrations respond to the FT aerosol concentration. Figure 4c shows the domain-mean salt number concentration directly above the surface in the lowest model level (solid lines) as well as the average cloud droplet concentration (dashed lines). As is expected, the simulations initialized with higher aerosol concentrations in the free troposphere also have higher concentrations in the boundary layer due to transport of aerosol into the BL via either activation of FT aerosol at cloud top and subsequent hydrometeor evaporation in the boundary layer or by direct transport from the FT without being activated Igel et al. (2017). In all cases the BL aerosol concentration (less than about 80 cm^{-3} for all simulations) remains an order of magnitude lower than what was initialized in the FT. Concentrations rapidly increase at the start of the simulations due to aerosol entrainment in salt600-salt1000. Eventually, aerosol concentrations decrease in time for all simulations, most likely due to dry and wet deposition and reduction in particle concentrations due to weak collision-coalescence. In salt20, without a large source of particles in the FT, surface concentrations are rapidly depleted within only a few hours after the simulations start. We note though that the rate of aerosol depletion in our simulations is likely unrealistically fast since our simulations lack sources of particles from the surface or from new particle formation.

The mean droplet concentration is very closely linked to the surface aerosol concentrations (Fig. 4c). As such, our simulations show an increase in droplet number concentration (N_d) and a decrease in mean droplet radius (r_d) with an increase in FT aerosol concentrations. Figure 5a shows profiles of N_d at various times throughout the simulation period. There is an approximate linear increase in the droplet concentration with the linearly increasing tropospheric aerosol concentrations. All profiles show a small increase in N_d at cloud top which becomes less prominent with time, consistent with the nucleation of a relatively high number of entrained aerosol particles at cloud top. The mean cloud droplet radius (Fig. 5b) decreases with increasing aerosol concentrations. In each simulation, cloud droplet number concentrations are decreasing and mean radii are increasing in time.
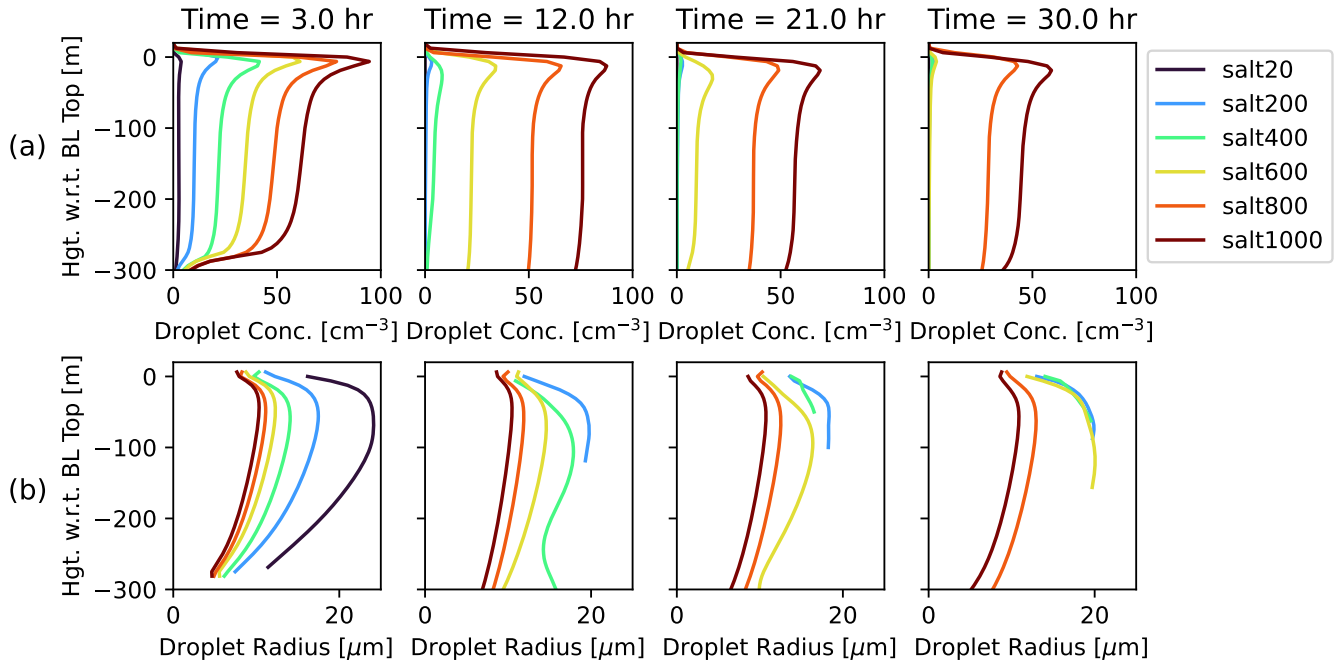
Figure 5. Evolution of (a) mean cloud droplet number concentration and (b) mass-mean cloud droplet radius profiles for all simulations every 9 hours. The y-axes display heights with respect to the boundary layer top.

This is indicative of either a decrease in the availability of CCN in the boundary layer and/or a decrease in the amount of aerosol being entrained into the cloud.

The result of the combined increase in cloud droplet number and decrease in radius is a reduction in collision coalescence efficiency. Figure 4c shows the rain water path (RWP) evolution for each simulation. There is clearly sensitivity to the tropospheric aerosol concentration with salt20 raining the most at the beginning of the simulation before dissipating. The peak rain rate is delayed as the FT aerosol increases and salt1000 produces almost no rain at all. Such precipitation suppression has been commonly described in response to increasing aerosol concentrations in both warm- and mixed-phase stratocumulus clouds (e.g. Albrecht, 1989; Wood, 2005; Peng et al., 2002). As noted above, although rain is being produced, very little rain actually reaches the surface.

While salt20 simulates an essentially complete removal of aerosol and cloud water, salt200 and salt400 do not simulate complete dissipation of the clouds. Rather, salt200 and salt400 simulate persistent, very thin clouds, less than 40 m thick and wih LWP < 5 g m^{-2} (Fig. 4a), with a very small number of relatively large droplets (< 1 cm^{-3} in number and 10-20 μm in radius; Fig. 5). Some of this water resides in the rain category, but we note that this rain water is produced when the droplets grow by condensation to exceed the maximum allowed mean cloud droplet diameter of 50 μm (not shown). In this situation, some cloud water is transferred to the rain category. Collision-coalescence is minimal. In this state, there are no longer strong sinks of aerosol number concentration since any particle that is activated can be returned to the atmosphere
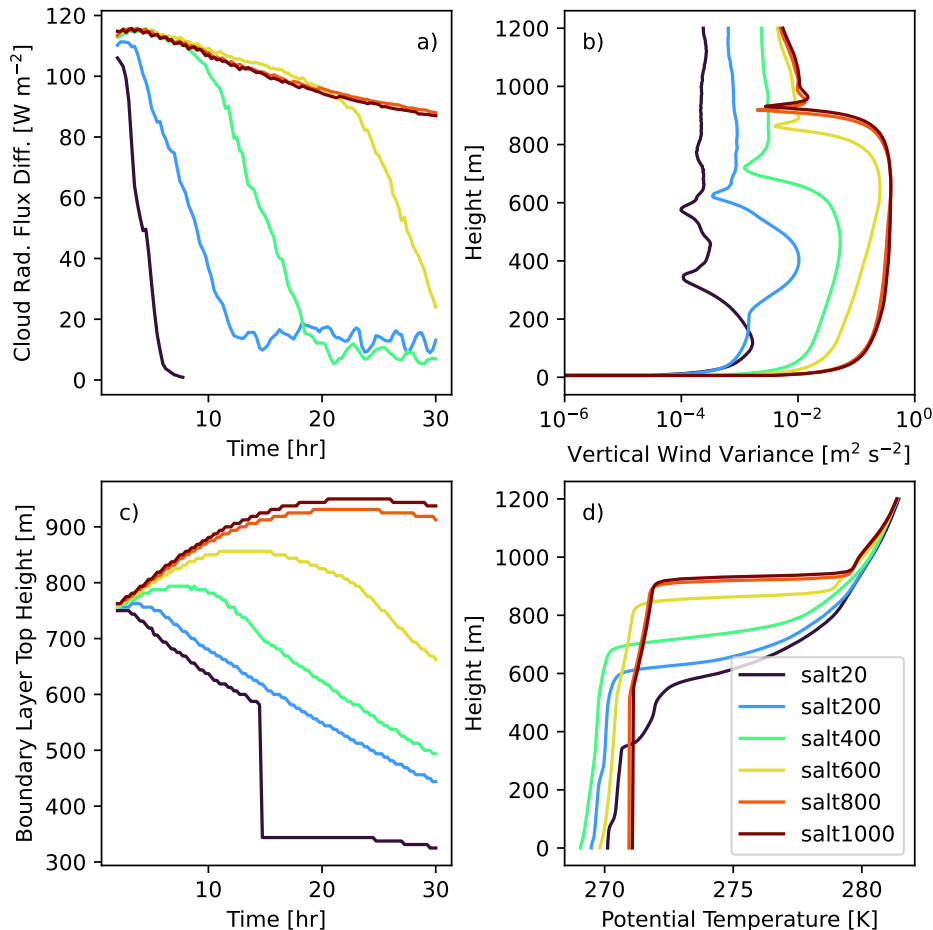
Figure 6. Time series of (a) radiative flux difference across the cloud layer and (c) boundary layer top height. Vertical profiles of (b) vertical wind variance (σ_w^2) and (d) boundary layer potential temperature (θ) at the hour 15.

upon drop evaporation. These thin clouds are still weakly turbulent. We do not know if such a state - one with very low LWP coincident with very low aerosol particle concentrations - commonly exists in the Arctic atmosphere. Certainly liquid-bearing clouds with LWP less than 25 g m^{-2} are frequently occurring (Silber et al., 2020; Sedlar, 2014). Alternatively, because the aerosol concentrations that are simulated are exceptionally low given our lack of particle sources in the model, the simulated clouds may not be representative of the Arctic atmosphere.

4.2 Thermodynamic Response

The precipitation suppression process is the primary factor in the spread in LWP seen in Figure 4a. However, it is not the only process impacting the LWP. As is expected, a change in a cloud's liquid water path also affects its emissivity. Figure 6a shows a time series of the net longwave radiative flux difference across the cloud layer. This difference is equivalent to the

vertically integrated longwave radiative cooling occurring in the cloud layer. There is a large spread in the flux difference, with
around 80 W m^{-2} separating salt600 and above from salt20 and salt200 around hour 20. This radiative sensitivity to aerosol
concentration is triggered first by the precipitation suppression effect described above. The less numerous, larger droplets
created with fewer aerosol lead to the development of thin clouds with less liquid water, which do not behave as a blackbody
but rather as a graybody. This radiative behavior of thin water clouds is consistent with previous work (Morrison et al., 2008;
Shupe and Intrieri, 2004; Mauritsen et al., 2011; Garrett and Zhao, 2006). While generally longwave impacts of the aerosol
indirect effects are seen as minimal (especially in thicker stratocumulus clouds in lower latitude), Morrison et al. (2008) found
through modeling that changing aerosol concentrations had a longwave effect in thin clouds with LWP $<$ 50 g m^{-2}. Shupe
and Intrieri (2004) have a lower threshold of 30 g m^{-2} for this effect. Our results are consistent with these previous studies.
Salt400, with its LWP of 50 g m^{-2} or less throughout most of the simulation, has an integrated radiative cooling that differs
substantially from those for salt600 and above.

This longwave sensitivity is important since, in the absence of surface fluxes, the cloud must be maintained from the top-
down (cooling at cloud top drives an overturning buoyancy circulation) versus the from bottom-up (surface heat fluxes and BL
instability drive vertical motions). As such, the dynamics of the cloud are sensitive to changes in radiative cooling rates within
the cloud layer. The much reduced cooling rates in the salt200 and salt400 clouds contribute to the reduced LWP. At the same
time, the reduced cooling rates help to maintain these clouds in their low LWP state by helping to reduce rain formation.

The vertical wind variance, which is the vertical component of turbulence kinetic energy (TKE) $\sigma_w^2 = \overline{w'w'}$, thus also has
a sensitivity to the tropospheric aerosol concentrations. Figure 6b shows the domain-average vertical profile of σ_w^2 midway
through the simulations. Simulations with higher aerosol concentrations drive stronger average vertical motions. The effect of
increasing aerosol concentrations on vertical motions is more apparent at lower aerosol concentrations, where the clouds are
thinner and increasing cloud droplet concentration and LWP has a stronger effect on the longwave emissivity of the cloud. As
clouds start to approach a blackbody in salt600 and above, the difference in σ_w^2 becomes smaller.

These changes to the turbulent mixing have consequences for the development of the boundary layer. Figure 6c shows the
evolution of boundary layer top height (defined as the height with maximum curvature in the potential temperature profile)
with time. In the higher aerosol simulations (salt800/salt1000), the BL top is nearly constant in time after about hour 15 (by
design). On the other extreme, salt20 develops a second inversion at the base of the dissipating cloud. Around hour 15, this
inversion becomes stronger than the original inversion and our diagnosed BL top plummets from around 600 m to around 350
m. This double inversion structure in salt20 is seen explicitly in the potential temperature profile at hour 15 (Fig. 6d). Salt200
and salt400 do not have a total collapse of the cloudy mixed layer, but they do have rapidly descending BL tops accompanied
by weakened temperature inversions (Fig. 6d). With surface fluxes disabled and without a cloud-driven circulation to drive
entrainment, the large-scale subsidence will act to lower the height of the inversion and a lack of mixing will weaken the
inversion.

Finally, the collapsing of the boundary layer has implications for aerosol entrainment and ultimately for the cloud's ability to
maintain itself. Successful entrainment of tropospheric aerosol depends on a layer of enhanced aerosol concentration directly
above the mixed layer. Figure 7 shows that in salt200 and salt600 (and salt400, but not shown), a buffer develops between the
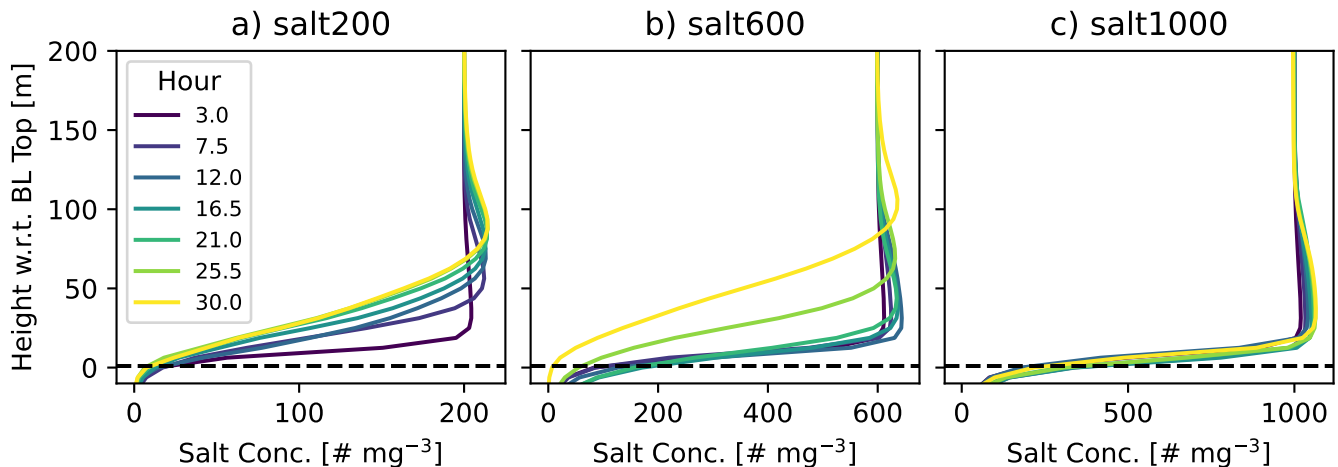
Figure 7. Profiles of aerosol concentrations near the boundary layer top for salt200, salt600, and salt1000.

aerosol in the FT and the top of the boundary layer. In these simulations, the boundary layer is collapsing which leaves behind a layer of air with aerosol concentrations that are much lower than those is the rest of the free troposphere. In salt800 and above, the boundary layer top is maintained and is better able to stay in contact with the tropospheric aerosol reservoir. This is a likely factor in the faster decrease of BL aerosol concentrations in the salt20-salt400 simulations seen in Figure 4c, and, more importantly, in the ability of clouds to sustain themselves in the face of very low boundary layer aerosol concentrations. As a result of the weakened turbulent mixing, the low FT salt simulations effectively cut themselves off from the reservoir of particles in the free troposphere.

4.3 Sensitivity Tests

Finally, we briefly look at the thermodynamic sensitivity tests that we ran. Salt400 reaches a nearly dissipated state in all but the test with the moderate inversion (MODINV), albeit the cloud water desiccation occurs more slowly than in the BASE set up (Fig. 8a). Longer cloud maintenance with a weaker inversion is unsurprising since the entrainment of aerosol particles should be faster. Indeed, we see that salt400-MODINV and salt1000-MODINV have the highest droplet concentrations (Fig. 8c,g) and that these are sufficient to suppress the rain water path (Fig. 8b,f). Salt400-MODINV is also the most successful in keeping the FT aerosol reservoir in contact with the boundary layer top, whereas the other salt400 tests show varying degrees of separation between the two (Fig. 8d). Salt1000 is much more sensitive to the initial thermodynamic conditions (Fig. 8e-g) than salt400. Most importantly though, in all tests the cloud is maintained throughout the simulation and good contact is kept between the boundary layer top and the aerosol reservoir (Fig. 8f). While certainly more time could be spent examining these tests, the primary point is that in the absence of other aerosol sources, a concentration of 400 cm^{-3} in the free troposphere may or may not be sufficient to maintain a cloud, whereas a concentration of 1000 cm^{-3} appears more likely to be frequently sufficient,
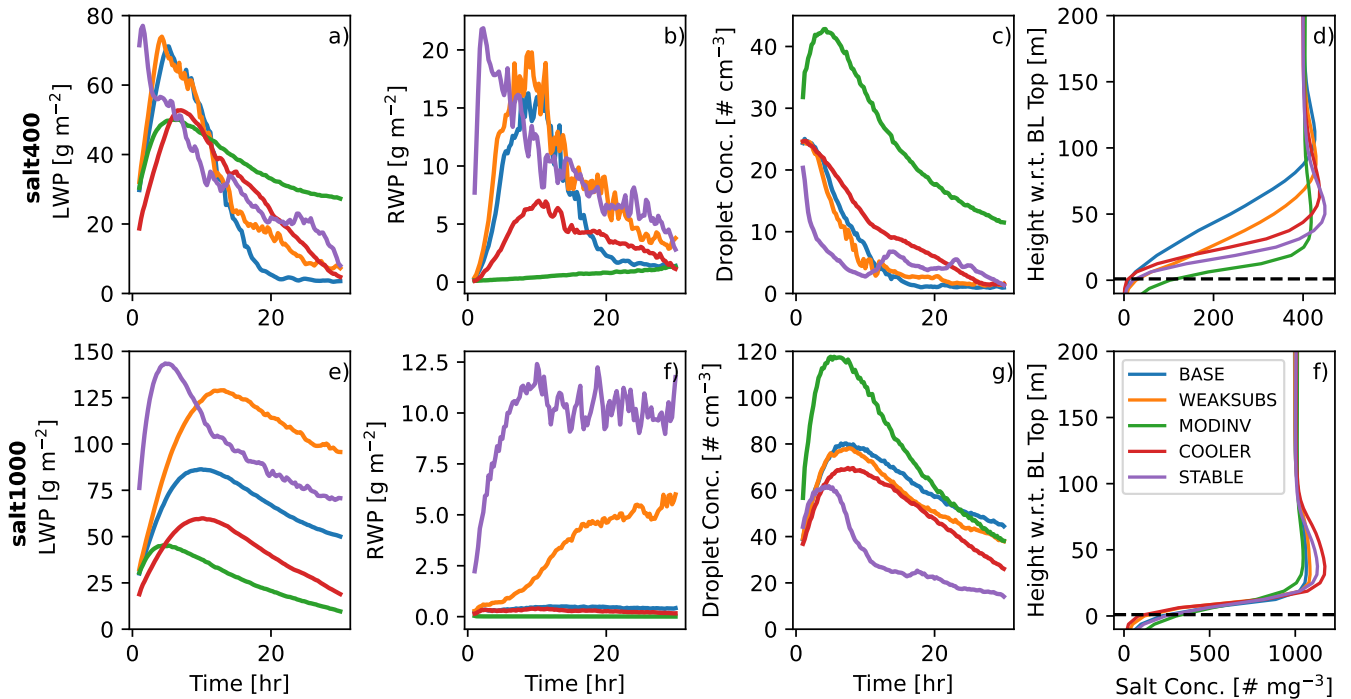
Figure 8. (a,e) Liquid water path time series, (b,f) rain water path time series, (c,g) mean cloud droplet number concentrations time series, and (d,f) salt concentration profiles at hour 30 for (a-d) salt400 sensitivity tests and (e-f) salt1000 sensitivity tests. The first two hours are omitted.

and that the processes that we describe in detail above that lead to the cloud desiccation appear to be occurring under these alternative thermodynamic conditions as well.

5   Conclusions

We present idealized LES simulations of an Arctic low-level cloud with various tropospheric aerosol concentrations (which serve only as CCN). A baseline simulation with low aerosol concentration (20 mg^{-1} of salt) in both the boundary layer and free troposphere simulated a cloud that was unable to sustain itself more than a few hours. Increasing tropospheric salt concentrations from 200 - 1000 mg^{-1} (in multiples of 200 mg^{-1}) increasing LWP. The lower aerosol concentration simulations yielded clouds that either dissipated within the simulation period or persisted with very low LWP. The higher aerosol concentration simulations produced clouds that maintained high LWP throughout all or most of the simulation period.

The cloud sensitivity to aerosol in the free troposphere is a result of entrainment and activation of aerosol particles from the troposphere into the cloud layer. This process causes three feedbacks that result in the change in liquid water content in the cloud:

285   – Increasing tropospheric aerosol concentrations leads to the commonly noted precipitation suppression effect. As more aerosol are entrained into the cloud layer and activated, the available liquid is divided among more droplets, causing an increase in cloud droplet number and a decrease in their size. This results in a less efficient collision-coalescence processes and thus less removal of water by rain.

    – As a consequence of the rain suppression the higher liquid water content in the higher aerosol concentration simulations
290   causes stronger cooling at cloud top. This cooling, which is primarily responsible for the circulations that maintain the cloud in the absence of surface forcing, drives stronger vertical motions in the clouds with higher droplet concentrations.

    – Finally, due to these two processes, higher FT aerosol concentration simulations are better able to maintain contact between the FT aerosol reservoir and the boundary layer top in order to maintain the very aerosol entrainment that supports the precipitation suppression.

295   We find that tropospheric aerosol concentrations of more than 400 mg^{-1} were necessary for cloud persistence beyond about 24 hours in most of the conditions that we tested. This concentration is only meant to be a very rough estimate which will of course depend on thermodynamic conditions and the size and hygroscopicity of the aerosol particles (which was rather high with our assumed salt particles). Nonetheless, it is encouraging that such concentrations are well within the range generally found in the lower free troposphere (Fig. 1b and e.g. Lonardi et al., 2022; Jung et al., 2018). Given that the required
300 concentrations are realistic, continuous aerosol entrainment from the FT is likely important in the summertime high Arctic for maintaining low-level clouds. As discussed in the introduction, others have speculated that Aitken particles are important for explaining cloud maintenance under low aerosol conditions and found evidence of Aitken particle activation in these clouds (Bulatovic et al., 2021; Karlsson et al., 2021, 2022; Siegel et al., 2022). Here we present a second mechanism for maintaining a sufficient CCN supply that can work together with Aitken particle activation. A major limitation of this study is that we did
305 not include new particle formation in our simulations. Price et al. (2023) found that in the late summer in the Arctic boundary layer there is a transition from particle sources dominated by long-range transport and entrainment through the boundary layer top to local new particle formation. As such, there is reason to believe that new particle formation may be important at this time of year. We also did not include Aitken particles in our simulations. Future work looking at the maintenance of clouds under low aerosol conditions should consider all of these processes.

310 *Code and data availability.* Tethered balloon data can be found on PANGAEA: meteorology data Pilz et al. (2022b), aerosol data Pilz et al. (2022a), broadband longwave radiation Lonardi et al. (2022a), and liquid water flags Lonardi et al. (2022b). Model source code and namelists used in this study can be found at https://doi.org/10.5281/zenodo.7991354 (Sterzinger et al., 2023). Horizontally-averaged processed model data used for analysis can be found at https://doi.org/10.5281/zenodo.7986917 (Sterzinger and Igel, 2023b). Code used to generate plots for this paper can be found at https://doi.org/10.5281/zenodo.7996595 (Sterzinger and Igel, 2023a).

315 *Author contributions.* LJS and ALI conceived the study. LJS and ALI conducted and analyzed the simulations. ALI analyzed the tethered balloon data. LJS wrote the original draft. LJS and ALI edited and reviewed the draft.

Competing interests. The authors declare no competing interests.

Acknowledgements. We thank two anonymous reviewers for their comments on the manuscript. This research was supported by the U.S. Department of Energy's Atmospheric System Research, an Office of Science Biological and Environmental Research program, under Grant 320 No. DE-SC0019073-0.

References

Albrecht, B. A.: Aerosols, Cloud Microphysics, and Fractional Cloudiness, Science, 245, 1227–1230, https://doi.org/10.1126/science.245.4923.1227, 1989.

Bulatovic, I., Igel, A. L., Leck, C., Heintzenberg, J., Riipinen, I., and Ekman, A. M. L.: The Importance of Aitken Mode Aerosol Particles for Cloud Sustenance in the Summertime High Arctic – a Simulation Study Supported by Observational Data, Atmospheric Chemistry and Physics, 21, 3871–3897, https://doi.org/10.5194/acp-21-3871-2021, 2021.

Cotton, W. R., Pielke Sr., R. A., Walko, R. L., Liston, G. E., Tremback, C. J., Jiang, H., McAnelly, R. L., Harrington, J. Y., Nicholls, M. E., Carrio, G. G., and McFadden, J. P.: RAMS 2001: Current Status and Future Directions, Meteorology and Atmospheric Physics, 82, 5–29, https://doi.org/10.1007/s00703-001-0584-9, 2003.

Creamean, J. M., de Boer, G., Telg, H., Mei, F., Dexheimer, D., Shupe, M. D., Solomon, A., and McComiskey, A.: Assessing the Vertical Structure of Arctic Aerosols Using Balloon-Borne Measurements, Atmospheric Chemistry and Physics, 21, 1737–1757, https://doi.org/10.5194/acp-21-1737-2021, 2021.

Deardorff, J. W.: Stratocumulus-Capped Mixed Layers Derived from a Three-Dimensional Model, Boundary-Layer Meteorol, 18, 495–527, https://doi.org/10.1007/BF00119502, 1980.

DeMott, P. J., Prenni, A. J., Liu, X., Kreidenweis, S. M., Petters, M. D., Twohy, C. H., Richardson, M. S., Eidhammer, T., and Rogers, D. C.: Predicting Global Atmospheric Ice Nuclei Distributions and Their Impacts on Climate, Proceedings of the National Academy of Sciences, 107, 11 217–11 222, https://doi.org/10.1073/pnas.0910818107, 2010.

Garrett, T. J. and Zhao, C.: Increased Arctic Cloud Longwave Emissivity Associated with Pollution from Mid-Latitudes, Nature, 440, 787–789, https://doi.org/10.1038/nature04636, 2006.

Hegg, D. A., Ferek, R. J., and Hobbs, P. V.: Cloud Condensation Nuclei over the Arctic Ocean in Early Spring, Journal of Applied Meteorology and Climatology, 34, 2076–2082, https://doi.org/10.1175/1520-0450(1995)034<2076:CCNOTA>2.0.CO;2, 1995.

Heintzenberg, J., Leck, C., and Tunved, P.: Potential Source Regions and Processes of Aerosol in the Summer Arctic, Atmospheric Chemistry and Physics, 15, 6487–6502, https://doi.org/10.5194/acp-15-6487-2015, 2015.

Igel, A. L., Ekman, A. M. L., Leck, C., Tjernström, M., Savre, J., and Sedlar, J.: The Free Troposphere as a Potential Source of Arctic Boundary Layer Aerosol Particles, Geophysical Research Letters, 44, 7053–7060, https://doi.org/10.1002/2017GL073808, 2017.

Intrieri, J. M., Fairall, C. W., Shupe, M. D., Persson, P. O. G., Andreas, E. L., Guest, P. S., and Moritz, R. E.: An Annual Cycle of Arctic Surface Cloud Forcing at SHEBA, Journal of Geophysical Research: Oceans, 107, SHE 13–1–SHE 13–14, https://doi.org/10.1029/2000JC000439, 2002.

Jozef, G. C., Cassano, J. J., Dahlke, S., Dice, M., Cox, C. J., and de Boer, G.: Thermodynamic and kinematic drivers of atmospheric boundary layer stability in the central Arctic during the Multidisciplinary drifting Observatory for the Study of Arctic Climate (MOSAiC), Atmospheric Chemistry and Physics, 23, 13 087–13 106, https://doi.org/10.5194/acp-23-13087-2023, 2023.

Jung, C. H., Yoon, Y. J., Kang, H. J., Gim, Y., Lee, B. Y., Ström, J., Krejci, R., and Tunved, P.: The Seasonal Characteristics of Cloud Condensation Nuclei (CCN) in the Arctic Lower Troposphere, Tellus B: Chemical and Physical Meteorology, 70, 1–13, https://doi.org/10.1080/16000889.2018.1513291, 2018.

Karlsson, L., Krejci, R., Koike, M., Ebell, K., and Zieger, P.: A long-term study of cloud residuals from low-level Arctic clouds, Atmospheric Chemistry and Physics, 21, 8933–8959, https://doi.org/10.5194/acp-21-8933-2021, publisher: Copernicus GmbH, 2021.

Karlsson, L., Baccarini, A., Duplessis, P., Baumgardner, D., Brooks, I. M., Chang, R. Y.-W., Dada, L., Dällenbach, K. R., Heikki-
nen, L., Krejci, R., Leaitch, W. R., Leck, C., Partridge, D. G., Salter, M. E., Wernli, H., Wheeler, M. J., Schmale, J., and
Zieger, P.: Physical and Chemical Properties of Cloud Droplet Residuals and Aerosol Particles During the Arctic Ocean 2018
360   Expedition, Journal of Geophysical Research: Atmospheres, 127, e2021JD036 383, https://doi.org/10.1029/2021JD036383, _eprint:
https://onlinelibrary.wiley.com/doi/pdf/10.1029/2021JD036383, 2022.

Kecorius, S., Vogl, T., Paasonen, P., Lampilahti, J., Rothenberg, D., Wex, H., Zeppenfeld, S., van Pinxteren, M., Hartmann, M., Henning,
S., Gong, X., Welti, A., Kulmala, M., Stratmann, F., Herrmann, H., and Wiedensohler, A.: New particle formation and its effect on cloud
condensation nuclei abundance in the summer Arctic: a case study in the Fram Strait and Barents Sea, Atmospheric Chemistry and Physics,
365   19, 14 339–14 364, https://doi.org/10.5194/acp-19-14339-2019, 2019.

Klein, S. A., McCoy, R. B., Morrison, H., Ackerman, A. S., Avramov, A., de Boer, G., Chen, M., Cole, J. N., del Genio, A. D., Falk, M.,
Foster, M. J., Fridlind, A., Golaz, J. C., Hashino, T., Harrington, J. Y., Hoose, C., Khairoutdinov, M. F., Larson, V. E., Liu, X., Luo,
Y., McFarquhar, G. M., Menon, S., Neggers, R. A., Park, S., Poellot, M. R., Schmidt, J. M., Sednev, I., Shipway, B. J., Shupe, M. D.,
Spangenberg, D. A., Sud, Y. C., Turner, D. D., Veron, D. E., von Salzen, K., Walker, G. K., Wang, Z., Wolf, A. B., Xie, S., Xu, K. M., Yang,
370   F., and Zhang, G.: Intercomparison of Model Simulations of Mixed-Phase Clouds Observed during the ARM Mixed-Phase Arctic Cloud
Experiment. I: Single-layer Cloud, Quarterly Journal of the Royal Meteorological Society, 135, 979–1002, https://doi.org/10.1002/qj.416,
2009.

Koike, M., Ukita, J., Ström, J., Tunved, P., Shiobara, M., Vitale, V., Lupi, A., Baumgardner, D., Ritter, C., Hermansen, O., Yamada, K.,
and Pedersen, C. A.: Year-Round In Situ Measurements of Arctic Low-Level Clouds: Microphysical Properties and Their Relation-
375   ships With Aerosols, Journal of Geophysical Research: Atmospheres, 124, 1798–1822, https://doi.org/10.1029/2018JD029802, _eprint:
https://onlinelibrary.wiley.com/doi/pdf/10.1029/2018JD029802, 2019.

Lonardi, M., Pilz, C., Akansu, E. F., Dahlke, S., Egerer, U., Ehrlich, A., Griesche, H., Heymsfield, A. J., Kirbus, B., Schmitt, C. G., Shupe,
M. D., Siebert, H., Wehner, B., and Wendisch, M.: Tethered Balloon-Borne Profile Measurements of Atmospheric Properties in the
Cloudy Atmospheric Boundary Layer over the Arctic Sea Ice during MOSAiC: Overview and First Results, Elementa: Science of the
380   Anthropocene, 10, 000 120, https://doi.org/10.1525/elementa.2021.000120, 2022.

Lonardi, M., Pilz, C., Siebert, H., Ehrlich, A., and Wendisch, M.: Tethered balloon-borne measurements of terrestrial radiation during
MOSAiC leg 4 in July 2020, https://doi.org/10.1594/PANGAEA.944200, 2022a.

Lonardi, M., Pilz, C., Siebert, H., Ehrlich, A., and Wendisch, M.: Tethered balloon-borne measurements of liquid cloud water presence during
MOSAiC leg 4 in July 2020, https://doi.org/10.1594/PANGAEA.944068, 2022b.

385   Mauritsen, T., Sedlar, J., Tjernstrom, M., Leck, C., Martin, M., Shupe, M., Sjögren, S., Sierau, B., Persson, P. O. G., and Brooks, I. M.: An
Arctic CCN-limited Cloud-Aerosol Regime, Atmospheric Chemistry and Physics, 11, 165–173, 2011.

McCoy, I. L., Bretherton, C. S., Wood, R., Twohy, C. H., Gettelman, A., Bardeen, C. G., and Toohey, D. W.: Influences of Recent Parti-
cle Formation on Southern Ocean Aerosol Variability and Low Cloud Properties, Journal of Geophysical Research: Atmospheres, 126,
e2020JD033 529, https://doi.org/10.1029/2020JD033529, _eprint: https://onlinelibrary.wiley.com/doi/pdf/10.1029/2020JD033529, 2021.

390   Meyers, M. P., Walko, R. L., Harrington, J. Y., and Cotton, W. R.: New RAMS Cloud Microphysics Parameterization. Part II: The Two-
Moment Scheme, Atmospheric Research, 45, 3–39, https://doi.org/10.1016/S0169-8095(97)00018-5, 1997.

Morrison, H., Pinto, J. O., Curry, J. A., and McFarquhar, G. M.: Sensitivity of Modeled Arctic Mixed-Phase Stratocumulus to Cloud Conden-
sation and Ice Nuclei over Regionally Varying Surface Conditions: SIMULATION OF ARCTIC MIXED-PHASE CLOUDS, J. Geophys.
Res., 113, n/a–n/a, https://doi.org/10.1029/2007JD008729, 2008.

395   Morrison, H., McCoy, R. B., Klein, S. A., Xie, S., Luo, Y., Avramov, A., Chen, M., Cole, J. N. S., Falk, M., Foster, M. J., Del Genio, A. D., Harrington, J. Y., Hoose, C., Khairoutdinov, M. F., Larson, V. E., Liu, X., McFarquhar, G. M., Poellot, M. R., von Salzen, K., Shipway, B. J., Shupe, M. D., Sud, Y. C., Turner, D. D., Veron, D. E., Walker, G. K., Wang, Z., Wolf, A. B., Xu, K.-M., Yang, F., and Zhang, G.: Intercomparison of Model Simulations of Mixed-Phase Clouds Observed during the ARM Mixed-Phase Arctic Cloud Experiment. II: Multilayer Cloud, Quarterly Journal of the Royal Meteorological Society, 135, 1003–1019, https://doi.org/10.1002/qj.415, 2009.

400   Morrison, H., Zuidema, P., Ackerman, A. S., Avramov, A., De Boer, G., Fan, J., Fridlind, A. M., Hashino, T., Harrington, J. Y., Luo, Y., Ovchinnikov, M., and Shipway, B.: Intercomparison of Cloud Model Simulations of Arctic Mixed-Phase Boundary Layer Clouds Observed during SHEBA/FIRE-ACE, Journal of Advances in Modeling Earth Systems, 3, https://doi.org/10.1029/2011MS000066, 2011.

Morrison, H., De Boer, G., Feingold, G., Harrington, J., Shupe, M. D., and Sulia, K.: Resilience of Persistent Arctic Mixed-Phase Clouds, Nature Geoscience, 5, 11–17, https://doi.org/10.1038/ngeo1332, 2012.

405   Peng, Y., Lohmann, U., Leaitch, R., Banic, C., and Couture, M.: The Cloud Albedo-Cloud Droplet Effective Radius Relationship for Clean and Polluted Clouds from RACE and FIRE.ACE: EVIDENCE FOR INDIRECT AEROSOL EFFECT, J. Geophys. Res., 107, AAC 1–1– AAC 1–6, https://doi.org/10.1029/2000JD000281, 2002.

Pilz, C., Lonardi, M., Siebert, H., and Wehner, B.: Tethered balloon-borne measurements of aerosol particle microphysics during the MO-SAiC expedition from June to July 2020, https://doi.org/10.1594/PANGAEA.943907, 2022a.

410   Pilz, C., Siebert, H., and Lonardi, M.: Tethered balloon-borne measurements of meteorological parameters during MOSAiC leg 4 in June and July 2020, https://doi.org/10.1594/PANGAEA.952341, 2022b.

Price, R., Baccarini, A., Schmale, J., Zieger, P., Brooks, I. M., Field, P., and Carslaw, K. S.: Late summer transition from a free-tropospheric to boundary layer source of Aitken mode aerosol in the high Arctic, Atmospheric Chemistry and Physics, 23, 2927–2961, https://doi.org/10.5194/acp-23-2927-2023, publisher: Copernicus GmbH, 2023.

415   Saleeby, S. M. and Cotton, W. R.: A Large-Droplet Mode and Prognostic Number Concentration of Cloud Droplets in the Colorado State University Regional Atmospheric Modeling System (RAMS). Part I: Module Descriptions and Supercell Test Simulations, Journal of Applied Meteorology, 43, 182–195, https://doi.org/10.1175/1520-0450(2004)043<0182:ALMAPN>2.0.CO;2, 2004.

Saleeby, S. M. and van den Heever, S. C.: Developments in the CSU-RAMS Aerosol Model: Emissions, Nucleation, Regeneration, Deposition, and Radiation, Journal of Applied Meteorology and Climatology, 52, 2601–2622, https://doi.org/10.1175/JAMC-D-12-0312.1,
420   2013.

Schröder, D., Vihma, T., Kerber, A., and Brümmer, B.: On the parameterization of turbulent surface fluxes over heterogeneous sea ice surfaces, Journal of Geophysical Research: Oceans, 108, https://doi.org/https://doi.org/10.1029/2002JC001385, 2003.

Sedlar, J.: Implications of Limited Liquid Water Path on Static Mixing within Arctic Low-Level Clouds, Journal of Applied Meteorology and Climatology, 53, 2775 – 2789, https://doi.org/https://doi.org/10.1175/JAMC-D-14-0065.1, 2014.

425   Sedlar, J., Tjernström, M., Mauritsen, T., Shupe, M. D., Brooks, I. M., Persson, P. O. G., Birch, C. E., Leck, C., Sirevaag, A., and Nicolaus, M.: A Transitioning Arctic Surface Energy Budget: The Impacts of Solar Zenith Angle, Surface Albedo and Cloud Radiative Forcing, Clim Dyn, 37, 1643–1660, https://doi.org/10.1007/s00382-010-0937-5, 2011.

Shupe, M. D.: Clouds at Arctic Atmospheric Observatories. Part II: Thermodynamic Phase Characteristics, Journal of Applied Meteorology and Climatology, 50, 645–661, https://doi.org/10.1175/2010JAMC2468.1, 2011.

430   Shupe, M. D. and Intrieri, J. M.: Cloud Radiative Forcing of the Arctic Surface: The Influence of Cloud Properties, Surface Albedo, and Solar Zenith Angle, Journal of Climate, 17, 616–628, https://doi.org/10.1175/1520-0442(2004)017<0616:CRFOTA>2.0.CO;2, 2004.

Shupe, M. D., Matrosov, S. Y., and Uttal, T.: Arctic Mixed-Phase Cloud Properties Derived from Surface-Based Sensors at SHEBA, Journal of the Atmospheric Sciences, 63, 697–711, https://doi.org/10.1175/JAS3659.1, 2006.

Shupe, M. D., Walden, V. P., Eloranta, E., Uttal, T., Campbell, J. R., Starkweather, S. M., and Shiobara, M.: Clouds at Arctic Atmospheric Observatories. Part I: Occurrence and Macrophysical Properties, J. Appl. Meteor. Climatol., 50, 626–644, https://doi.org/10.1175/2010JAMC2467.1, 2011.

Shupe, M. D., Rex, M., Blomquist, B., Persson, P. O. G., Schmale, J., Uttal, T., Althausen, D., Angot, H., Archer, S., Bariteau, L., Beck, I., Bilberry, J., Bucci, S., Buck, C., Boyer, M., Brasseur, Z., Brooks, I. M., Calmer, R., Cassano, J., Castro, V., Chu, D., Costa, D., Cox, C. J., Creamean, J., Crewell, S., Dahlke, S., Damm, E., de Boer, G., Deckelmann, H., Dethloff, K., Dütsch, M., Ebell, K., Ehrlich, A., Ellis, J., Engelmann, R., Fong, A. A., Frey, M. M., Gallagher, M. R., Ganzeveld, L., Gradinger, R., Graeser, J., Greenamyer, V., Griesche, H., Griffiths, S., Hamilton, J., Heinemann, G., Helmig, D., Herber, A., Heuzé, C., Hofer, J., Houchens, T., Howard, D., Inoue, J., Jacobi, H.-W., Jaiser, R., Jokinen, T., Jourdan, O., Jozef, G., King, W., Kirchgaessner, A., Klingebiel, M., Krassovski, M., Krumpen, T., Lampert, A., Landing, W., Laurila, T., Lawrence, D., Lonardi, M., Loose, B., Lüpkes, C., Maahn, M., Macke, A., Maslowski, W., Marsay, C., Maturilli, M., Mech, M., Morris, S., Moser, M., Nicolaus, M., Ortega, P., Osborn, J., Pätzold, F., Perovich, D. K., Petäjä, T., Pilz, C., Pirazzini, R., Posman, K., Powers, H., Pratt, K. A., Preußer, A., Quéléver, L., Radenz, M., Rabe, B., Rinke, A., Sachs, T., Schulz, A., Siebert, H., Silva, T., Solomon, A., Sommerfeld, A., Spreen, G., Stephens, M., Stohl, A., Svensson, G., Uin, J., Viegas, J., Voigt, C., von der Gathen, P., Wehner, B., Welker, J. M., Wendisch, M., Werner, M., Xie, Z., and Yue, F.: Overview of the MOSAiC expedition: Atmosphere, Elementa: Science of the Anthropocene, 10, https://doi.org/10.1525/elementa.2021.00060, _eprint: https://online.ucpress.edu/elementa/article-pdf/10/1/00060/780058/elementa.2021.00060.pdf, 2022.

Siegel, K., Neuberger, A., Karlsson, L., Zieger, P., Mattsson, F., Duplessis, P., Dada, L., Daellenbach, K., Schmale, J., Baccarini, A., Krejci, R., Svenningsson, B., Chang, R., Ekman, A. M. L., Riipinen, I., and Mohr, C.: Using Novel Molecular-Level Chemical Composition Observations of High Arctic Organic Aerosol for Predictions of Cloud Condensation Nuclei, Environmental Science & Technology, 56, 13 888–13 899, https://doi.org/10.1021/acs.est.2c02162, publisher: American Chemical Society, 2022.

Silber, I., Fridlind, A. M., Verlinde, J., Russell, L. M., and Ackerman, A. S.: Nonturbulent Liquid-Bearing Polar Clouds: Observed Frequency of Occurrence and Simulated Sensitivity to Gravity Waves, Geophysical Research Letters, 47, e2020GL087 099, https://doi.org/10.1029/2020GL087099, 2020.

Sotiropoulou, G., Sedlar, J., Forbes, R., and Tjernstrom, M.: Summer Arctic Clouds in the ECMWF Forecast Model: An Evaluation of Cloud Parametrization Schemes, Quarterly Journal of the Royal Meteorological Society, 142, 387–400, https://doi.org/10.1002/qj.2658, 2016.

Stephens, G. L., Gabriel, P. M., and Partain, P. T.: Parameterization of Atmospheric Radiative Transfer. Part I: Validity of Simple Models, Journal of the Atmospheric Sciences, 58, 3391–3409, https://doi.org/10.1175/1520-0469(2001)058<3391:POARTP>2.0.CO;2, 2001.

Sterzinger, L. and Igel, A.: Plotting Scripts for Sterzinger and Igel (2023), https://doi.org/10.5281/zenodo.7996595, 2023a.

Sterzinger, L. and Igel, A. L.: Model data for Sterzinger and Igel (2023) "Simulated Idealized Arctic Cloud Sensitivity to Above Cloud CCN Concentrations", https://doi.org/10.5281/zenodo.7986917, 2023b.

Sterzinger, L., Igel, A., and RAMS-Developers: Model source code and namelists for Sterzinger and Igel (2023), https://doi.org/10.5281/zenodo.7991355, 2023.

Sterzinger, L. J., Sedlar, J., Guy, H., Neely III, R. R., and Igel, A. L.: Do Arctic Mixed-Phase Clouds Sometimes Dissipate Due to Insufficient Aerosol? Evidence from Comparisons between Observations and Idealized Simulations, Atmospheric Chemistry and Physics, 22, 8973–8988, https://doi.org/10.5194/acp-22-8973-2022, 2022.

Stevens, R. G., Loewe, K., Dearden, C., Dimitrelos, A., Possner, A., Eirund, G. K., Raatikainen, T., Hill, A. A., Shipway, B. J., Wilkinson, J., Romakkaniemi, S., Tonttila, J., Laaksonen, A., Korhonen, H., Connolly, P., Lohmann, U., Hoose, C., Ekman, A. M., Carslaw, K. S., and Field, P. R.: A Model Intercomparison of CCN-limited Tenuous Clouds in the High Arctic, Atmospheric Chemistry and Physics, 18, 11 041–11 071, https://doi.org/10.5194/acp-18-11041-2018, 2018.

Verlinde, J., Harrington, J. Y., McFarquhar, G. M., Yannuzzi, V. T., Avramov, A., Greenberg, S., Johnson, N., Zhang, G., Poellot, M. R., Mather, J. H., Turner, D. D., Eloranta, E. W., Zak, B. D., Prenni, A. J., Daniel, J. S., Kok, G. L., Tobin, D. C., Holz, R., Sassen, K., Spangenberg, D., Minnis, P., Tooman, T. P., Ivey, M. D., Richardson, S. J., Bahrmann, C. P., Shupe, M., DeMott, P. J., Heymsfield, A. J., and Schofield, R.: The Mixed-Phase Arctic Cloud Experiment, Bull. Amer. Meteor. Soc., 88, 205–222, https://doi.org/10.1175/BAMS-88-2-205, 2007.

Willis, M. D., Burkart, J., Thomas, J. L., Köllner, F., Schneider, J., Bozem, H., Hoor, P. M., Aliabadi, A. A., Schulz, H., Herber, A. B., Leaitch, W. R., and Abbatt, J. P. D.: Growth of nucleation mode particles in the summertime Arctic: a case study, Atmospheric Chemistry and Physics, 16, 7663–7679, https://doi.org/10.5194/acp-16-7663-2016, publisher: Copernicus GmbH, 2016.

Wood, R.: Drizzle in Stratiform Boundary Layer Clouds. Part II: Microphysical Aspects, Journal of the Atmospheric Sciences, 62, 3034–3050, https://doi.org/10.1175/JAS3530.1, 2005.

Wyant, M. C., Bretherton, C. S., Wood, R., Blossey, P. N., and McCoy, I. L.: High Free-Tropospheric Aitken-Mode Aerosol Concentrations Buffer Cloud Droplet Concentrations in Large-Eddy Simulations of Precipitating Stratocumulus, Journal of Advances in Modeling Earth Systems, 14, e2021MS002 930, https://doi.org/10.1029/2021MS002930, _eprint: https://onlinelibrary.wiley.com/doi/pdf/10.1029/2021MS002930, 2022.

Wylie, D. P. and Hudson, J. G.: Effects of Long-Range Transport and Clouds on Cloud Condensation Nuclei in the Springtime Arctic, Journal of Geophysical Research: Atmospheres, 107, AAC 13–1–AAC 13–11, https://doi.org/10.1029/2001JD000759, 2002.